Chinese Journal of Structural Chemistry

COMMUNICATION

# Tuning Solvent Composition to Enhance the Stability of Metal Clusters in Mass Spectrometry

Yingzi Han[1], Yihuang Jiang[1], Jing Jeanne Yang[1]*, Shuichao Lin[1], Zichao Tang[1]* and Lansun Zheng[1]

[1]*State Key Laboratory of Physical Chemistry of Solid Surface, College of Chemistry and Chemical Engineering, Xiamen University, Xiamen 361005, China.*

**ABSTRACT** Electrospray ionization time-of-flight mass spectrometry (ESI-TOF-MS) has been recognized as a powerful technique for studying metal clusters' chemical composition and reaction mechanisms. It is a great challenge in mass spectrometry analysis to maintain the metal cluster molecules intact without fragmentation, which is achieved in this work by using mixed solvents to change the interaction between cluster molecules and solvent molecules, further affecting the fragmentation behaviors of the metal cluster in MS. Theoretical analysis reveals that the stability of the $[(C)Au_6Ag_2(C_{18}H_{14}ONP)_6]^{4+}$ cluster in ESI-TOF-MS is related to the strength of the chemical bonds between its own atoms and the bonding between the solvent and the cluster molecules.

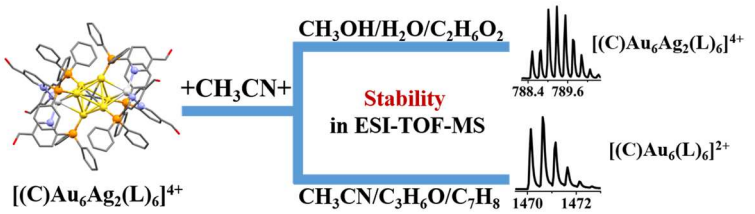


**Keywords:** metal cluster, mass spectrometry, fragmentation, stability, hydrogen bond

## INTRODUNTION

Ligand-protected atomically precise metal clusters have attracted more and more attention due to their unusual physiochemical properties associated with their unique electronic structures,[1,2] which have various potential applications in catalysis,[3-5] photoluminescence,[6-8] chirality,[9-11] magnetism,[12-14] bio-imaging,[15-17] chemical sensing,[18,19] nanomedicine,[20,21] energy and environment.[22,23] Due to the feature of well-defined structure and molecular composition, metal clusters have become ideal models to explore and comprehensively understand the surface science, structure-property correlations, growth mechanism and to realize rational design of complex nanomaterials at the atomic/molecular level.[1,24-26] As a molecular characterization technique, especially due to the characteristics of soft ionization, mass spectrometry (MS) with electrospray ionization (ESI) source[27,28] and matrix assisted laser desorption ionization (MALDI) source,[29,30] which can ionize of clusters directly from solution and from solid state respectively, has shown the significant effectiveness to characterize the composition[31,32] and gives insights into their chemical behaviors of metal clusters, such as growth mechanism,[25,33,34] ligand exchange,[35,36] fragmentation behaviors,[37] alloying and intercluster reactions.[38,39] However, because of the weak noncovalent interactions, such as coordination bonds and metal-metal bonds, metal clusters are easily decomposed during the ionization processes in MS analysis, and it is challenging to obtain intact molecular ion peaks of the clusters.[40,41] In 2008, Dass et al.[42] reported the first MALDI spectra of intact ligand-protected Au nanoclusters ($Au_{25}(SCH_2CH_2Ph)_{18}$) by using DCTB as a matrix which assists ionization through electron transfer, and successfully suppressed the extensive fragmentation in previous experiments to detect intact molecular ions. A different approach was explored by Su and co-workers in 2016,[43] who applied two types of ESI-MS analyzers to compare the MS behaviors of metal clusters, and demonstrated that time-of-flight (TOF) analyzer is easier to gain the intact cluster information than ion trap (IT) analyzer, but the latter could also have a chance to keep whole clusters intact without fragmentation by carefully optimizing the buffer gas and radiofrequency amplitude. However, there are relatively few studies on the stability of metal clusters in mass spectrometry environments.

In this contribution, a positive tetravalent bimetallic cluster $[(C)Au_6Ag_2(L)_6]^{4+}$ (L = 2-(diphenylphosphino)-5-pyridinecarboxaldehyde, with four "$BF_4^-$" as counter anions) is applied to compare

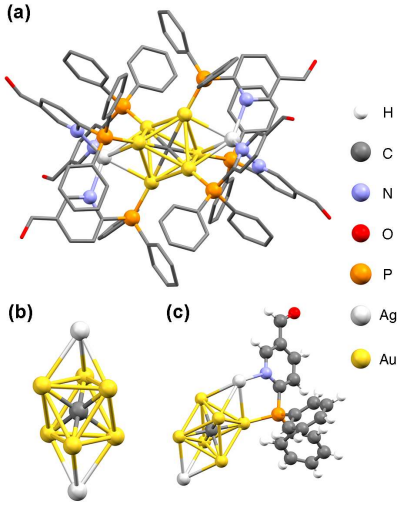


**Figure 1.** Representative crystal structure of the $[(C)Au_6Ag_2(L)_6]^{4+}$ cluster. (a) The full picture of the cluster structure, in which hydrogens are not displayed, and carbons and oxygens are displayed as a framework; (b) Structure of the $(C)Au_6Ag_2$ core; (c) Coordination bonds between the $(C)Au_6Ag_2$ core and one ligand L.

  
DOI: 10.14102/j.cnki.0254-5861.2022-0032

the MS fragmentation behaviors by high resolution (HR)-ESI-TOF-MS, especially the molecular ion peaks of the cluster under different solvent environments. We optimized the crystal structure of the cluster by *ab initio* calculation based on the published crystallographic information file (cif).[44] As shown in Figure 1, the cluster has a bicapped octahedral configuration which could be viewed as the fusion of two $Au_3Ag$ moieties sharing a carbon center (C). In a $Au_3Ag$ moiety, each Au atom is connected to a L ligand by forming Au-P coordination bond, and the Ag atom is wrapped by three pyridyl groups of L ligands with Ag-N coordination bonds. Here we report a combined MS and theoretical work, finding that under given MS conditions, the fragmentation behaviors of this metal cluster are directly related to the relative strength of various chemical bonds.

## RESULTS AND DISCUSSION

**MS Behaviors of the Cluster in $CH_3CN$ and $CH_3CN$+$CH_3OH$ Solvents.** Figure 2a is the HR-ESI-TOF MS signal of the cluster crystal dissolved in $CH_3CN$. There shows a group of dominant peaks at m/z around 1470.6, together with a low intensity but still visible peak at m/z around 1016.4, which can be well assigned to $[(C)Au_6(L)_6]^{2+}$ and $[(C)Au_6Ag(L)_6]^{3+}$, respectively. These two observed ions are the fragments of the parent ion $[(C)Au_6Ag_2(L)_6]^{4+}$ via losing two or one $Ag^+$. The intact cluster ion ($[(C)Au_6Ag_2(L)_6]^{4+}$, m/z around 789.0) has not been detected in the spectrum. In contrast, as reported by Su et al.,[43] the similar metal clusters can remain intact in the ESI-TOF-MS experiment using the solvent of $CH_3OH$. It should be noted that the clusters we studied here cannot dissolve well in $CH_3OH$. Although TOF is believed to be a "soft" analyzer, the results indicate the solvent also has a great relationship with the stability of the cluster under TOF-MS conditions.

The above results show that the cluster dissolved in acetonitrile ($CH_3CN$) is prone to dissociate in the MS condition, leading the intact cluster ions to be not detected. However, when using a mixed solvent of $CH_3CN$ and $CH_3OH$ with equal volume, we obtained an obviously different mass spectrum, as shown in Figure 2b. Two sets of prominent ion peaks are clearly shown in the m/z range of 1000 to 1600. The set with a smaller m/z contains five positive trivalent ion peaks, and the interval between each adjacent peak is 10.7. Similarly, the set with a larger m/z involves six positive divalent ion peaks, with the interval to be 16.0. The above two sets of peaks are composed of two series of peaks with exactly the same mass difference of 32.0, corresponding to the molecular weight of $CH_3OH$. Thus, we believe the six L ligands containing aldehyde groups (L = RCHO, R = $PPh_2C_5H_3N$, as illustrated in Figure 2a) in the original cluster underwent varying degrees of hemiacetal reaction with the solvent molecule $CH_3OH$, and transformed to hemiacetal ligands $L_\alpha$ ($L_\alpha$ = RHC(OH)($OCH_3$), as illustrated in Figure 2b). This structure was further confirmed by the infrared (IR) spectroscopy (see Figure S1). The IR peak at 1712 $cm^{-1}$ which represents the vibrational mode of C=O group almost disappears when $CH_3OH$ is applied as the mixed solvent, implying the occurrence of hemiacetal reaction. Therefore, the two sets of peaks mentioned above can be assigned to $[(C)Au_6Ag(L)_{4\sim0}(L_\alpha)_{2\sim6}]^{3+}$ and $[(C)Au_6(L)_{5\sim0}(L_\alpha)_{1\sim6}]^{2+}$, respectively. One can also see in Figure 2b that, unlike the MS behavior using pure $CH_3CN$ solvent, the MS peak intensity of trivalent ions increased significantly when using a mixed solvent of $CH_3CN$ and $CH_3OH$, even slightly exceeding the peak intensity of divalent ions. More importantly, the intact cluster ion peaks have been observed in Figure 2b at m/z around 820 to 840. The enlarged details of the peaks are shown in Figure 2c, together with the well matched simulation results of these isotopic patterns. With the adding of $CH_3OH$ into $CH_3CN$, the probability of $Ag^+$ dissociation from the clusters has been greatly reduced under MS conditions. Although the intensity of these peaks is relatively low, the ability to detect complete molecular ion peaks is of great significance in MS characterizations.

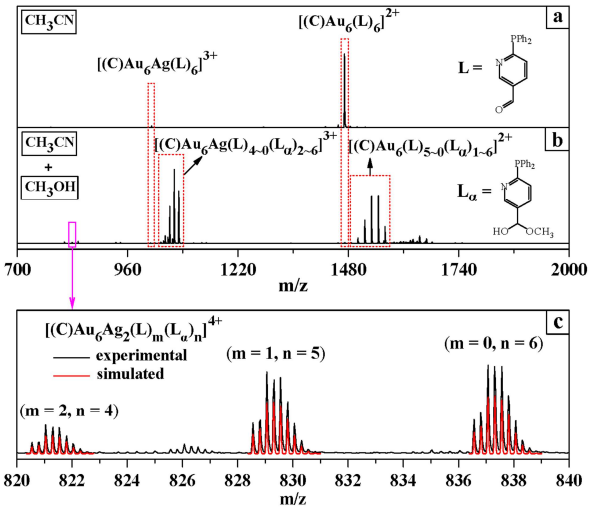


**Figure 2.** Mass spectra obtained by HR-ESI-TOF-MS of the $[(C)Au_6Ag_2(L)_6]^{4+}$ cluster dissolved in (a) $CH_3CN$; (b) Mixed solvent of $CH_3CN$ and $CH_3OH$ in equal volume. (c) Enlarged details of (b) in the m/z range of 820 to 840, which show both experimental (black) and simulated (red) isotopic patterns of the molecular ion peaks of $[(C)Au_6Ag_2(L)_m(L_\alpha)_n]^{4+}$.

**Hydrogen Bond Effect on the MS Behavior of Clusters.** Whether $Ag^+$ in the $[(C)Au_6Ag_2(L)_6]^{4+}$ cluster tends to dissociate under MS conditions depends largely on the type of solvent. As the commonly used solvent in cluster characterization, $CH_3CN$ aggravates the dissociation of $Ag^+$ in the cluster. However, with the participation of $CH_3OH$ and formation of hydrogen bond with $CH_3CN$, the dissociation of $Ag^+$ is greatly suppressed. A detailed mechanism will be discussed in the next section. Based on the above facts, here we propose a strategy to control the MS stability of metal clusters. Feasibility of this strategy has been further validated by another four solvents, by mixing $CH_3CN$ with water ($H_2O$), ethylene glycol ($C_2H_6O_2$), acetone ($C_3H_6O$), and toluene ($C_7H_8$), respectively. Only the first two mixed solvent molecules can form hydrogen bonds with $CH_3CN$. Since ethylene glycol has a high viscosity, a mixing ratio of $V(C_2H_6O_2)$:$V(CH_3CN)$ = 1:4 is adopted in order to achieve a smooth MS testing. For other three types of mixed solvents, the two components are prepared in an equal volume. The mass spectra obtained under the same detection conditions are displayed in Figure 3. As we expected, after adding $H_2O$ (Figure 3a) or $C_2H_6O_2$ (Figure 3b), the molecular ion peaks containing intact cluster structure "$(C)Au_6Ag_2$" can




DOI: 10.14102/j.cnki.0254-5861.2022-0032

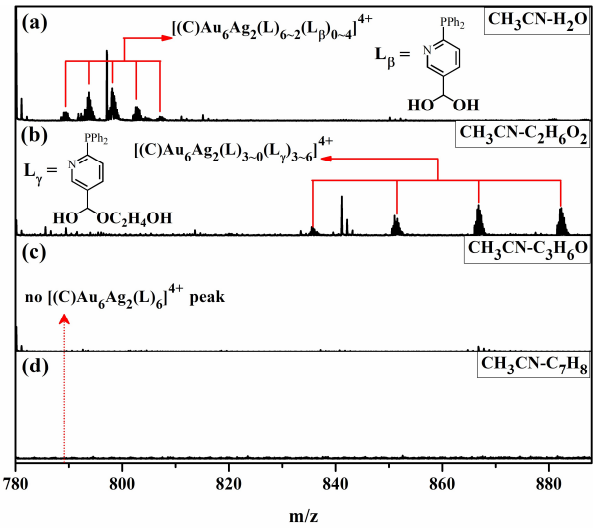


**Figure 3.** Mass spectra obtained by HR-ESI-TOF-MS of the $[(C)Au_6Ag_2(L)_6]^{4+}$ cluster dissolved in mixed solvents of $CH_3CN$ with (a) $H_2O$, (b) $C_2H_6O_2$, (c) $C_3H_6O$, and (d) $C_7H_8$ in equal volumes (except for $C_2H_6O_2$ with $V(C_2H_6O_2):V(CH_3CN)$ = 1:4), respectively.

be successfully detected. Due to the occurrence of hemiacetal reactions, the original six L ligands were converted into the hemiacetal products $L_\beta$ or $L_\gamma$ to a certain extent (shown in the Figure for the molecular structures). In contrast, no molecular ion peaks were detected when $C_3H_6O$ (Figure 3c) or $C_7H_8$ (Figure 3d) was added. These results further illustrate that the important influence of hydrogen bonds on the coordination bonds of metal clusters will lead to significant changes in their dissociation behaviors in MS.

**Analysis and Discussion.** According to Figure 2, the apparent differences in dissociation behavior of the cluster in MS under two different solvents prompt us to reconsider the influence of the solvent molecules on the cluster structure. As shown in Figure 1b, the metal core of the cluster is a regular octahedron composed of six Au atoms, together with two Ag atoms on two opposite surfaces. Each Au atom is coordinated to the P atom of a ligand, and each Ag atom is coordinated with the N atoms on the three ligands. Here the strength of these chemical bonds was evaluated based on the relative level of molecular orbital energies. Figure 4a shows the strongest molecular orbital between Au and P atoms, which is bonded from $5d_{z^2}$ orbital of the Au atoms and 3*s*/3*p* orbitals of the P atoms. Figure 4b depicts the strongest molecular orbital between Ag and N atoms, formed through the 4*d* orbital of the Ag atom and the $\pi$ orbital on the N-containing heterocyclic ring. Figure 4c shows a discrete orbital containing the bonding properties between the $4d_{z^2}$ orbital of the Ag atom and 5*d* orbitals of the three Au atoms (See Figure S2 for the enlarged part of Ag and Au). The energy levels of these molecular orbitals are –0.481, –0.214 and –0.182 a.u., respectively, relative to the HOMO. It is obvious that the Au atoms are tightly bonded to the central C and surrounding P atoms, while Ag atoms are weakly bonded to the "$(C)Au_6$" core as well as the ligands. This explains why the dominate signals in Figure 2 correspond to cluster fragments with all six ligands, and only one or two Ag atoms are dissociated from the cluster. The acetonitrile molecules can promote the dissociation of Ag from the cluster because the coordination strength with Ag atoms is stronger than that between N and Ag in the cluster, which leads to the dissolution of Ag atoms in acetonitrile. Take the simplest case where only one $CH_3CN$ molecule reacts with the cluster, a complex ion like $\{(C)Au_6Ag(L)_6[(N,N)\text{-}Ag\text{-}NCCH_3]\}^{4+}$ may be generated, in which "(N,N)-Ag" represents that only two N atoms from two L ligands form coordination bonds with the Ag atom. In this complex, one of the Ag–N bonds between Ag and one ligand in the original cluster is broken and Ag–N bond between Ag and the attacking $CH_3CN$ molecule is newly formed. The computed overall enthalpy for the formation of this complex is +0.48 kcal/mol ($T_l$ = 298 K) in the acetonitrile solution. Although slightly endothermic, we can calculate from the Maxwell-Boltzmann rule that about 30% of the original clusters will exist in such a complex form in the thermodynamic equilibrium acetonitrile solution. In contrast, the above reaction has an enthalpy of –15.84 kcal/mol in the gas phase ($T_g$ = 423 K), indicating a very favorable thermodynamic driving force in the MS condition. Furthermore, the complex is unstable in the mass spectrometer due to strong electric field, and will further loose the "$(Ag\text{-}NCCH_3)^+$" fraction via Coulomb explosion, leaving the structurally stable $[(C)Au_6Ag(L)_6]^{3+}$ component to be detected. Similarly, the other $Ag^+$ can also be lost, resulting in the detected $[(C)Au_6(L)_6]^{2+}$ signal as shown in Figure 2a. In fact, we successfully captured the fragment ion $[Ag(L)(CH_3CN)]^+$ in MS experiments (see Figure S3), which should come from the dissociation of $\{(C)Au_6Ag(L)_6[(N,N)\text{-}Ag\text{-}NCCH_3]\}^{4+}$ with binding one ligand from surrounding environment.

Hydrogen bond interactions between solvent molecules are believed to have a significant impact on the intact cluster information by MS. According to Figure 2b, after adding methanol

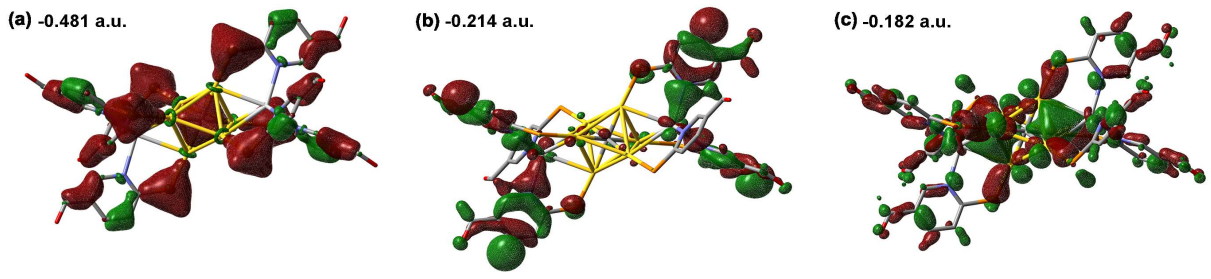


**Figure 4.** Molecular orbitals and corresponding energy levels of the chemical bond between (a) Au–P, (b) Ag–N, and (c) Au–Ag. Hydrogens and phenyls are not displayed for clarity.




DOI: 10.14102/j.cnki.0254-5861.2022-0032

solvent, the fragmentation tendency of the cluster was obviously suppressed, indicating that methanol molecules inhibited the coordination interaction between acetonitrile molecules and the cluster. The hydrogen bond strength between $CH_3CN$ and $CH_3OH$ is 5.02 kcal/mol from theoretical computations. Considering the $CH_3CN\cdots CH_3OH$ hydrogen bond breaking and the $\{(C)Au_6Ag(L)_6[(N,N)\text{-}Ag\text{-}NCCH_3]\}^{4+}$ complex forming processes together, the chance of complex formation is reduced, and the intact cluster is more likely to be retained under the subsequent MS conditions.

## CONCLUSION

In this work, we found that the metal cluster $[(C)Au_6Ag_2(L)_6]^{4+}$ easily dissociated two $Ag^+$ into $[(C)Au_6(L)_6]^{2+}$ fragments during ESI-TOF-MS analysis, which has been proved by molecular orbital studies of the cluster finding the weak Au–Ag and Ag–N bonding interactions in the cluster. However, we can adjust the solvent composition, and further interfere the interaction between metal clusters and solvent molecules, to weaken the dissociation tendency of Ag ions from the cluster and to obtain the intact molecular ions in mass spectrometry. These results have contributed greatly to our deeper understanding into the structure and bonding of the noncovalent metal cluster system. Mass spectrometry shows powerful capabilities in studying metal clusters and their reactions.

## EXPERIMENTAL

**Materials and Chemicals.** All reagents used in this work were commercially available and used without further purification. HPLC-grade acetonitrile and methanol were purchased from Spectrum Co. (New Brunswick, NJ, USA). Ethylene glycol (AR), acetone (AR), and toluene (AR) were bought from Sinopharm Chemical Reagent Co. (Shanghai, China). Ultrapure water was produced by laboratory water purification system.

**Sample Preparation.** The metal cluster $[(C)Au_6Ag_2(L)_6]^{4+}$ was prepared in a synthetic procedure according to the literature.[44] The cluster was dissolved in $CH_3CN$ to obtain a solution at $1\times10^{-5}$ mol/L (0.035 mg samples in 1 mL $CH_3CN$). As for mixed solvents, except for the 1:4 volume ratio of $C_2H_6O_2$ and $CH_3CN$, the others ($CH_3OH$, $H_2O$, $C_3H_6O$, $C_7H_8$) are mixed in equal volumes.

**Mass Spectrometric Analysis.** The mass spectrometric analysis was performed on a high-resolution electrospray ionization time-of-flight mass spectrometer (6224, Agilent, Santa Clara, CA, USA) in the positive-ion mode. The instrument was calibrated with an ESI tuning mix (Agilent) before MS analysis. The sample was introduced by a syringe pump (KDS-100, KD Scientific, Holliston, MA, USA) at a rate of 20 μL/min. Typical parameters used for the measurements were as follows. Capillary voltage: 4.0 kV; Drying gas temp: 150 ℃; Drying gas flow: 4 L/min; Nebulizer pressure: 20 psig.

**Computational Method.** The hydrogen bond energies, enthalpy change of the cluster dissociation process, and the molecular orbital levels of the cluster were computed using the Gaussian 09 Rev. D01 software.[45] All computations were performed with the doubly hybrid density functional theory of XYGJ-OS.[46] The LANL2DZ basis set for Au, Ag and 6-31G(d) basis set for O, C, H, P and N were used in geometry optimizations and harmonic frequencies, and def2-TZVP together with 6-311+G(d) basis set was used for transition metals and main group elements, respectively, in single point energy calculations.

## ACKNOWLEDGEMENTS

This work was supported by the National Natural Science Foundation of China (Nos. 91961107, 21827801, 21805231). We also thank Dr. Yang Yang (School of Chemistry and Materials Science, Jiangsu Normal University) for his assistance in sample preparation and Dr. Jun Chen (Fujian Institute of Research on the Structure of Matter, Chinese Academy of Sciences) for discussion in theoretical computations.

## AUTHOR INFORMATION

Corresponding authors. Emails: j.yang@xmu.edu.cn (Jing Jeanne Yang) and zctang@xmu.edu.cn (Zichao Tang)

## COMPETING INTERESTS

The authors declare no competing interests.

## ADDITIONAL INFORMATION

Supplementary information is available for this paper at http://manu30.magtech.com.cn/jghx/EN/10.14102/j.cnki.0254-5861.2022-0032

For submission: https://mc03.manuscriptcentral.com/cjsc

## REFERENCES

(1) Jin, R.; Zeng, C.; Zhou, M.; Chen, Y. Atomically precise colloidal metal nanoclusters and nanoparticles: fundamentals and opportunities. *Chem. Rev.* 2016, 116, 10346–10413.

(2) Du, Y.; Sheng, H.; Astruc, D.; Zhu, M. Atomically precise noble metal nanoclusters as efficient catalysts: a bridge between structure and properties. *Chem. Rev.* **2020**, 120, 526–622.

(3) Wang, S.; Jin, S.; Yang, S.; Chen, S.; Song, Y.; Zhang, J.; Zhu, M. Total structure determination of surface doping $[Ag_{46}Au_{24}(SR)_{32}](BPh_4)_2$ nanocluster and its structure-related catalytic property. *Sci. Adv.* **2015**, 1, e1500441.

(4) Wang, Y.; Wan, X. K.; Ren, L.; Su, H.; Li, G.; Malola, S.; Lin, S.; Tang, Z.; Häkkinen, H.; Teo, B. K.; Wang, Q. M.; Zheng, N. Atomically precise alkynyl-protected metal nanoclusters as a model catalyst: observation of promoting effect of surface ligands on catalysis by metal nanoparticles. *J. Am. Chem. Soc.* **2016**, 138, 3278–3281.

(5) Wan, X. K.; Wang, J. Q.; Nan, Z. A.; Wang, Q. M. Ligand effects in catalysis by atomically precise gold nanoclusters. *Sci. Adv.* **2017**, 3, e1701823.

(6) Ghosh, R.; Goswami, U.; Ghosh, S. S.; Paul, A.; Chattopadhyay, A. Synergistic anticancer activity of fluorescent copper nanoclusters and cisplatin delivered through a hydrogel nanocarrier. ACS *Appl. Mater. Interfaces* **2015**, 7, 209–222.

(7) Kang, X.; Zhu, M. Tailoring the photoluminescence of atomically precise nanoclusters. *Chem. Soc. Rev.* **2019**, 48, 2422–2457.

(8) Chang, H.; Karan, N. S.; Shin, K.; Bootharaju, M. S.; Nah, S.; Chae, S. I.; Baek, W.; Lee, S.; Kim, J.; Son, Y. J.; Kang, T.; Ko, G.; Kwon, S. H.; Hyeon, T. Highly fluorescent gold cluster assembly. *J. Am. Chem. Soc.*




DOI: 10.14102/j.cnki.0254-5861.2022-0032

**2021**, 143, 326–334.
(9) Zeng, C.; Li, T.; Das, A.; Rosi, N. L.; Jin, R. Chiral structure of thiolate-protected 28-gold-atom nanocluster determined by X-ray crystallography. *J. Am. Chem. Soc.* **2013**, 135, 10011–10013.
(10) Knoppe, S.; Wong, O. A.; Malola, S.; Hakkinen, H.; Burgi, T.; Verbiest, T.; Ackerson, C. J. Chiral phase transfer and enantioenrichment of thiolate-protected $Au_{102}$ clusters. *J. Am. Chem. Soc.* **2014**, 136, 4129–4132.
(11) Dolamic, I.; Varnholt, B.; Burgi, T. Chirality transfer from gold nanocluster to adsorbate evidenced by vibrational circular dichroism. *Nat. Commun.* **2015**, 6, 7117.
(12) Zhu, M.; Aikens, C. M.; Hendrich, M. P.; Gupta, R.; Qian, H.; Schatz, G. C.; Jin, R. Reversible switching of magnetism in thiolate-protected $Au_{25}$ superatoms. *J. Am. Chem. Soc.* **2009**, 131, 2490–2492.
(13) Antonello, S.; Perera, N. V.; Ruzzi, M.; Gascon, J. A.; Maran, F. Interplay of charge state, lability, and magnetism in the molecule-like $Au_{25}(SR)_{18}$ cluster. *J. Am. Chem. Soc.* **2013**, 135, 15585–15594.
(14) Hartmann, M. J.; Millstone, J. E.; Häkkinen, H. Surface chemistry controls magnetism in cobalt nanoclusters. *J. Phys. Chem. C* **2016**, 120, 20822–20827.
(15) Shang, L.; Azadfar, N.; Stockmar, F.; Send, W.; Trouillet, V.; Bruns, M.; Gerthsen, D.; Nienhaus, G. U. One-pot synthesis of near-infrared fluorescent gold clusters for cellular fluorescence lifetime imaging. *Small* **2011**, 7, 2614–2620.
(16) Raut, S. L.; Fudala, R.; Rich, R.; Kokate, R. A.; Chib, R.; Gryczynski, Z.; Gryczynski, I. Long lived BSA Au clusters as a time gated intensity imaging probe. *Nanoscale* **2014**, 6, 2594–2597.
(17) Zheng, K.; Yuan, X.; Goswami, N.; Zhang, Q.; Xie, J. Recent advances in the synthesis, characterization, and biomedical applications of ultrasmall thiolated silver nanoclusters. *RSC Adv.* **2014**, 4, 60581–60596.
(18) Xie, J.; Zheng, Y.; Ying, J. Y. Highly selective and ultrasensitive detection of $Hg^{2+}$ based on fluorescence quenching of Au nanoclusters by $Hg^{2+}$-$Au^{+}$ interactions. *Chem. Commun.* **2010**, 46, 961–963.
(19) Roy, S.; Palui, G.; Banerjee, A. The as-prepared gold cluster-based fluorescent sensor for the selective detection of $As^{III}$ ions in aqueous solution. *Nanoscale* **2012**, 4, 2734–2740.
(20) Wang, Y.; Wang, Y.; Zhou, F.; Kim, P.; Xia, Y. Protein-protected Au clusters as a new class of nanoscale biosensor for label-free fluorescence detection of proteases. *Small* **2012**, 8, 3769–3773.
(21) Zheng, K.; Setyawati, M. I.; Leong, D. T.; Xie, J. Antimicrobial gold nanoclusters. *ACS Nano* **2017**, 11, 6904–6910.
(22) Bootharaju, M. S.; Pradeep, T. Investigation into the reactivity of unsupported and supported $Ag_7$ and $Ag_8$ clusters with toxic metal ions. *Langmuir* **2011**, 27, 8134–8143.
(23) Mathew, A.; Pradeep, T. Noble metal clusters: applications in energy, environment, and biology. *Part. Part. Syst. Char.* **2014**, 31, 1017–1053.
(24) Chakraborty, I.; Pradeep, T. Atomically precise clusters of noble metals: emerging link between atoms and nanoparticles. *Chem. Rev.* **2017**, 117, 8208–8271.
(25) Yao, Q.; Yuan, X.; Fung, V.; Yu, Y.; Leong, D. T.; Jiang, D. E.; Xie, J. Understanding seed-mediated growth of gold nanoclusters at molecular level. *Nat. Commun.* **2017**, 8, 927.
(26) Yan, J.; Teo, B. K.; Zheng, N. Surface chemistry of atomically precise coinage-metal nanoclusters: from structural control to surface reactivity and catalysis. *Acc. Chem. Res.* **2018**, 51, 3084–3093.
(27) Wan, X. K.; Cheng, X. L.; Tang, Q.; Han, Y. Z.; Hu, G.; Jiang, D. E.; Wang, Q. M. Atomically precise bimetallic $Au_{19}Cu_{30}$ nanocluster with an icosidodecahedral $Cu_{30}$ shell and an alkynyl-Cu interface. *J. Am. Chem. Soc.* **2017**, 139, 9451–9454.
(28) Yu, Y.; Yue, C.; Han, Y.; Zhang, C.; Zheng, M.; Xu, B.; Lin, S.; Li, J.; Kang, J. Si nanorod arrays modified with metal-organic segments as anodes in lithium ion batteries. *RSC Adv*. **2017**, 7, 53680–53685.
(29) Dass, A. Mass spectrometric identification of $Au_{68}(SR)_{34}$ molecular gold nanoclusters with 34-electron shell closing. *J. Am. Chem. Soc.* **2009**, 131, 11666–11667.
(30) Knoppe, S.; Dharmaratne, A. C.; Schreiner, E.; Dass, A.; Burgi, T. Ligand exchange reactions on $Au_{38}$ and $Au_{40}$ clusters: a combined circular dichroism and mass spectrometry study. *J. Am. Chem. Soc.* **2010**, 132, 16783–16789.
(31) Nie, H. H.; Han, Y. Z.; Tang, Z.; Yang, S. Y.; Teo, B. K. Hydride induced formation and optical properties of tetrahedral $[Cu_4(\mu_4\text{-}H)(\mu_2\text{-}X)_2(PPh_2Py)_4]^+$ clusters (X = Cl, Br; Py = pyridyl). *J. Clust. Sci.* **2018**, 29, 837–846.
(32) Shen, H.; Han, Y.; Wu, Q.; Peng, J.; Teo, B. K.; Zheng, N. Simple and selective synthesis of copper-containing metal nanoclusters using $(PPh_3)_2CuBH_4$ as reducing agent. *Small Methods* **2020**, 2000603.
(33) Luo, Z.; Nachammai, V.; Zhang, B.; Yan, N.; Leong, D. T.; Jiang, D. E.; Xie, J. Toward understanding the growth mechanism: tracing all stable intermediate species from reduction of Au(I)-thiolate complexes to evolution of $Au_{25}$ nanoclusters. *J. Am. Chem. Soc.* **2014**, 136, 10577–10580.
(34) Ji, B. Q.; Su, H. F.; Jagodič, M.; Jagličić, Z.; Kurmoo, M.; Wang, X. P.; Tung, C. H.; Cao, Z. Z.; Sun, D. Self-organization into preferred sites by $Mg^{II}$, $Mn^{II}$, and $Mn^{III}$ in brucite-structured $M_{19}$ cluster. *Inorg. Chem.* **2019**, 58, 3800−3806.
(35) Bootharaju, M. S.; Joshi, C. P.; Alhilaly, M. J.; Bakr, O. M. Switching a nanocluster core from hollow to nonhollow. *Chem. Mater.* **2016**, 28, 3292–3297.
(36) Zhao, C.; Han, Y. Z.; Dai, S.; Chen, X.; Yan, J.; Zhang, W.; Su, H.; Lin, S.; Tang, Z.; Teo, B. K.; Zheng, N. Microporous cyclic titanium-oxo clusters with labile surface ligands. *Angew. Chem. Int. Ed.* **2017**, 56, 16252–16256.
(37) Roy, J.; Chakraborty, P.; Paramasivam, G.; Natarajan, G.; Pradeep, T. Gas phase ion chemistry of titanium-oxofullerene with ligated solvents. *Phys. Chem. Chem. Phys.* **2022**, 24, 2332–2343.
(38) Su, H.; Wang, Y.; Ren, L.; Yuan, P.; Teo, B. K.; Lin, S.; Zheng, L.; Zheng, N. Fractal patterns in nucleation and growth of icosahedral core of $[Au_nAg_{44-n}(SC_6H_3F_2)_{30}]4^-$ ($n$ = 0−12) via *ab initio* synthesis: continuously tunable composition control. *Inorg. Chem.* **2019**, 58, 259–264.
(39) Krishnadas, K. R.; Ghosh, A.; Baksi, A.; Chakraborty, I.; Natarajan, G.; Pradeep, T. Intercluster reactions between $Au_{25}(SR)_{18}$ and $Ag_{44}(SR)_{30}$. *J. Am. Chem. Soc.* **2016**, 138, 140–148.
(40) Harkness, K. M.; Cliffel, D. E.; McLean, J. A. Characterization of thiolate-protected gold nanoparticles by mass spectrometry. *Analyst* **2010**, 135, 868–874.
(41) Wang, Z.; Qu, Q. P.; Su, H. F.; Huang, P.; Gupta, R. K.; Liu, Q. Y.; Tung, C. H.; Sun, D.; Zheng, L. S. A novel 58-nuclei silver nanowheel encapsulating a subvalent $Ag_6^{4+}$ kernel. *Sci. China Chem.* **2020**, 63, 16–20.
(42) Dass, A.; Stevenson, A.; Dubay, G. R.; Tracy, J. B.; Murray, R. W. Nanoparticle MALDI-TOF mass spectrometry without fragmentation: $Au_{25}(SCH_2CH_2Ph)_{18}$ and mixed monolayer $Au_{25}(SCH_2CH_2Ph)_{18\text{-}x}(L)_x$. *J. Am. Chem. Soc.* **2008**, 130, 5940–5946.




DOI: 10.14102/j.cnki.0254-5861.2022-0032

(43) Su, H. F.; Yang, J. J.; Chen, Y.; Lin, S. C.; Zheng, L. S. Studying mass spectrometric behaviors of $\{Au_6Ag_2(C)[PPh_2(4\text{-}CH_3\text{-}Py)]_6\}(BF_4)_4$ and $\{Au_8[(PPh_3)_2O]_3(PPh_3)_2\}(NO_3)_2$ by electrospray time-of-flight mass spectrometry and electrospray ion trap mass spectrometry. *Rapid Commun. Mass Spectrom*. **2016**, 30, 8–13.

(44) Yang, Y.; Pei, X. L.; Wang, Q. M. Postclustering dynamic covalent modification for chirality control and chiral sensing. *J. Am. Chem. Soc.* **2013**, 135, 16184–16191.

(45) Frisch, M. J.; Trucks, G. W.; Schlegel, H. B.; Scuseria, G. E.; Robb, M. A.; Cheeseman, J. R.; Scalmani, G.; Barone, V.; Mennucci, B.; Petersson, G. A.; Nakatsuji, H.; Caricato, M.; Li, X.; Hratchian, H. P.; Izmaylov, A. F.; Bloino, J.; Zheng, G.; Sonnenberg, J. L.; Hada, M.; Ehara, M.; Toyota, K.; Fukuda, R.; Hasegawa, J.; Ishida, M.; Nakajima, T.; Honda, Y.; Kitao, O.; Nakai, H.; Vreven, T.; Montgomery, J. A. Jr.; Peralta, J. E.; Ogliaro, F.; Bearpark, M.; Heyd, J. J.; Brothers, E.; Kudin, K. N.; Staroverov, V. N.; Kobayashi, R.; Normand, J.; Raghavachari, K.; Rendell, A.; Burant J. C.; Iyengar S. S.; Tomasi, J.; Cossi, M.; Rega, N.; Millam, J. M.; Klene, M.; Knox, J. E.; Cross, J. B.; Bakken, V.; Adamo, C.; Jaramillo, J.; Gomperts, R.; Stratmann, R. E.; Yazyev, O.; Austin, A. J.; Cammi, R.; Pomelli, C.; Ochterski, J. W.; Martin, R. L.; Morokuma, K.; Zakrzewski, V. G.; Voth, G. A.; Salvador, P.; Dannenberg, J. J.; Dapprich, S.; Daniels, A. D.; Farkas, O.; Foresman, J. B.; Ortiz, J. V.; Cioslowski, J.; Fox, D. J. Gaussian 09 Revision D.01, Gaussian Inc. Wallingford CT **2009**.

(46) Zhang, I. Y.; Xu, X.; Jung, Y.; Goddard III, W. A. A fast doubly hybrid density functional method close to chemical accuracy using a local opposite spin ansatz. *Proc. Natl. Acad. Sci. USA* **2011**, 108, 19896–19900.

Received: February 17, 2022
Accepted: March 12, 2022
Published: April 8, 2022




DOI: 10.14102/j.cnki.0254-5861.2022-0032

SUPPORTING INFORMATION

Chinese Journal of Structural Chemistry

# Tuning Solvent Composition to Enhance the Stability of Metal Clusters in Mass Spectrometry

Yingzi Han[1], Yihuang Jiang[1], Jing Jeanne Yang[1]*, Shuichao Lin[1], Zichao Tang[1]* and Lansun Zheng[1]

[1]*State Key Laboratory of Physical Chemistry of Solid Surface, College of Chemistry and Chemical Engineering, Xiamen University, Xiamen 361005, China.*

*Corresponding authors. Emails: j.yang@xmu.edu.cn (Jing Jeanne Yang) and zctang@xmu.edu.cn (Zichao Tang)*

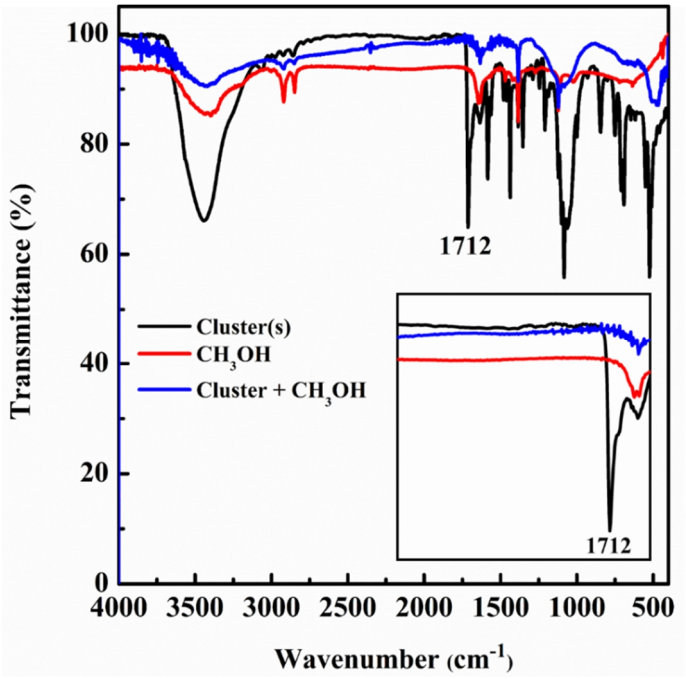


**Figure S1.** IR spectra of the cluster powders (black trace), $CH_3OH$ (red trace), the cluster dissolved in $CH_3OH$ (blue trace), respectively. Inset: the enlarged details in the range of 2300 to 1600 $cm^{-1}$. The C=O vibration peak at 1712 $cm^{-1}$ almost disappears when $CH_3OH$ is applied, implying the occurrence of hemiacetal reaction between the cluster ligands and solvent molecules.

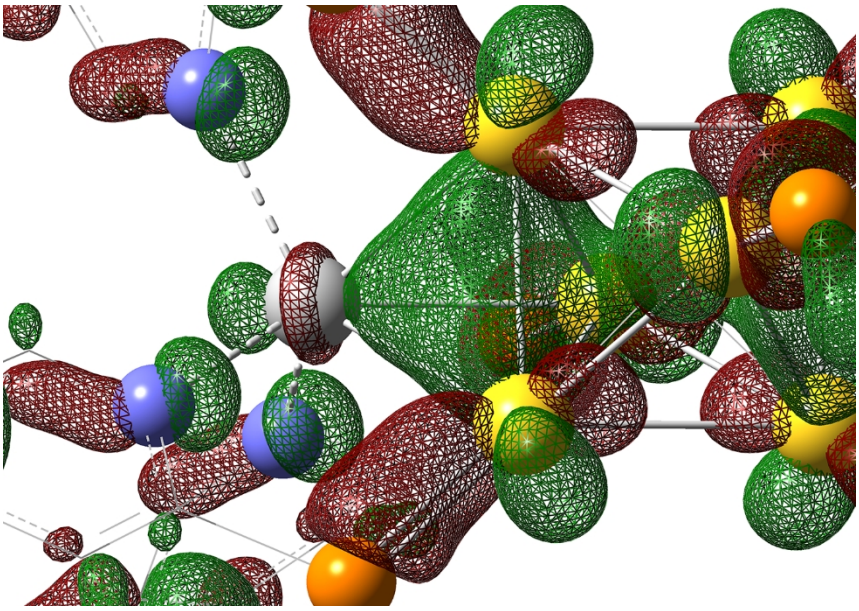

**Figure S2.** Enlarged part of Figure 4c illustrating the bonding properties between Ag and Au.

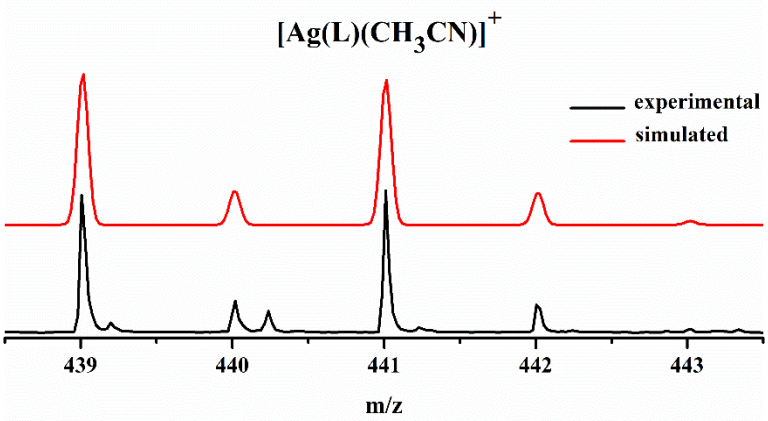


**Figure S3.** The experimental (black trace) and simulated (red trace) isotopic patterns of the fragment ion peak $[Ag(L)(CH_3CN)]^+$ obtained by HR-ESI-TOF-MS when the cluster dissolved in $CH_3CN$.